



# Recycling and utilization of agro-food waste ashes: syntheses of the glasses for wide-band gap semiconductor applications

Gaurav Sharma<sup>1</sup> · K. Singh<sup>1</sup>

Received: 3 August 2018 / Accepted: 20 January 2019 / Published online: 1 February 2019  
© Springer Japan KK, part of Springer Nature 2019

## Abstract

Present glasses are synthesized by the melt-quench method. The ashes of rice husk and sugarcane leaves are taken to synthesize the present samples. The eggshell powder is used to modify the glass-network and reduced the melting temperature of rice husk ash and sugarcane leaves ash. The as-quenched samples are characterized using different experimental techniques to study their structural and optical properties. The optical band gaps are found in the insulating range, i. e. 3.34–3.72 eV. The as-prepared glasses showed good luminescent properties due to some trace transition elements oxides present in the agro-food wastes. The agro-food wastes could be used as a resource and valuable materials to synthesize value-added engineering materials like glasses. The addition of eggshell powder into the main content showed the blue shift in photoluminescence spectra with enhanced intensity. This property may be exploited to develop UV–visible light-emitting diodes and some other non-linear optical devices.

**Keywords** Agro-food wastes · Continuous and pulsed laser applications · Glasses · Luminescence · Optical properties · X-ray diffraction

## Introduction

Silica is the most important inorganic chemical compounds [1] used for various applications in the engineering and medical sciences [2–4]. Usually, most of the silica is extracted from either chemical or metallurgical routes. These routes are time-consuming and expensive. On the other hand, naturally available silica, especially those found in agro-wastes, could be used as the resource materials for various applications [5]. The agro-food wastes are available in all countries, for instance, rice husk in most of the Asian countries and Brazil. On the other hand, eggshells are available all over the world [6–8], whereas other agro-food wastes like SCLA, corn husk and peanut shell are also produced, at large scale, as by-products in various countries like South Africa, France, Indonesia, Mexico, United Kingdom, Nigeria, USA, China and India, respectively [9–12]. The ever-growing amounts of the agricultural and food wastes are creating lot

of problems to the environment, which leads to the threat of intoxication to the humans and animals. Presently, agricultural and food wastes are being used as a fuel in the power plant and sugar factories, cattle food, rubber reinforcement and in construction of roads and buildings [13–15]. Recent time, efforts have been made to utilize these wastes as the new source of valuable and alternative materials [16–18]. It is reported that rice husk, dry sugarcane leaves and wheat straw ashes are containing a variable amount of silica with some trace elements [19–22]. The presence of high silica with variable amount of other oxides like CaO, MgO, Na<sub>2</sub>O, K<sub>2</sub>O, etc. could be used as an alternative source of conventional oxides for making glasses/glass–ceramics. Similarly, eggs are another basic food, which is consumed at a large scale all over the world. Mostly, the cover of eggs dumped as waste, has higher amount of CaO with some trace elements. This eggshell powder (ESP) can also be used as value-added products such as a bone substitute [23, 24].

Silicate-based glasses/glass–ceramics are being used for many applications like optical devices, window glasses, non-linear optics; renewable-energy production in solar cells and solid oxide fuels cells [25, 26]. Normally, required glasses are made by various high-purity commercially available chemicals such as SiO<sub>2</sub>, CaO, K<sub>2</sub>O, P<sub>2</sub>O<sub>5</sub>, Na<sub>2</sub>O, etc. [27].

✉ K. Singh  
kusingh@thapar.edu

<sup>1</sup> School of Physics and Materials Science, Thapar Institute of Engineering and Technology, 147004 Patiala, Punjab, India

Earlier, few researchers have reported that the well-known agro-food wastes could be used to synthesize the glasses [25, 28]. It is not only helpful to manage harmful wastes but also converted these wastes as the value-added materials for different engineering applications.

Moreover, Sigel et al. [29] suggested that the silicate glasses with some impurities like alkali and alkaline earth metals, and some other trace elements can be used as luminescent materials from 290 to 350 nm. Barbieri et al. [30] have reported the CaO–Al<sub>2</sub>O<sub>3</sub>–SiO<sub>2</sub> based glass–ceramics prepared from the agro-food wastes.

Based on above background, the calcined rice husk ash (RHA) and sugarcane leave ash (SCLA) contains very high content of silica [31–33]. On the other hand, ESP contains very high CaO [23]. As far as our knowledge, nobody use ESP to synthesize the glasses yet. The addition of ESP in calcined RHA and SCLA not only decrease the melting point but also modify the properties of the proposed glasses [34].

Therefore, proper and systematic addition of the eggshell powder at the cost of RHA constant weight percentage (wt%) of the SCLA has been used to prepare glasses/glass–ceramics. The as-prepared samples are characterized for their structural, optical and luminescence properties to investigate the possible use of resultant glasses/glass–ceramics in non-linear optics, device applications such as wide-band gap semiconductors and UV–visible light-emitting diode (LED).

## Materials and methods

### Sample preparation

Rice husk and dry sugarcane leaves were taken from the rice mills and agricultural fields, respectively. The proposed agricultural wastes and eggshells are mostly available in Asian, African and all over the world [10, 35]. These agricultural wastes were cleaned using acid and distilled water to remove the impurities. After proper drying, these wastes burnt in air to get fine ashes. Before making desirable samples, SCLA and RHA were heat-treated at 1000 °C for 12 h to remove organic impurities. On the other hand, the eggshell was collected from the poultry farm. Similarly, eggshell was also washed with distilled water followed by acid-treatment in a dilute solution of hydrochloric and nitric acid (1:1) to remove the adhering albumin and impurities.

Then, the eggshell was dried in an oven at 110 °C for 3 h and ground in an agate mortar-pestle to make the fine powder. The chemical compositions of these heat-treated waste ashes and label of samples are given in Tables 1 and 2, respectively. Ashes and eggshell powder were mixed and ground in an agate mortar-pestle to obtain homogenized powder. The homogenized mixture was kept at the programmable furnace for melting at 1550 °C. The melted samples were quenched on the solid copper plates. These samples were crushed using an agate mortar-pestle to get fine powder for further characterizations. Scanning electron microscope/energy dispersive spectroscopy (SEM/EDS) measurements were done to find the final composition of the as-quenched samples. These measurements were carried out by JOEL-JSM 6460 LV (Tokyo, JAPAN) microscope at the acceleration voltage of 15 kV. The samples were coated with the platinum (thickness 100 Å) to avoid electron charging. The density of the samples was calculated by Archimedes' principle in xylene using a sophisticated microbalance. The least count of the balance was 0.01 mg. The density of the samples was calculated as follows [36]:

$$\rho_{\text{sample}} = \frac{w_a}{w_a - w_x} \times \rho_x, \quad (1)$$

where  $\rho_{\text{sample}}$  is the density within the sample,  $w_a$  and  $w_x$  are the weight of the sample in air and in xylene.  $\rho_x$  is the density (0.863 g/cc) of xylene at room temperature. The structural properties of the samples was studied using X-ray diffraction on PANalytical X'Pert PROX-ray diffractometer with CuK<sub>α</sub> radiations ( $\lambda = 1.54 \text{ \AA}$ ). The scan rate and step size were  $\sim 3^\circ \text{ min}^{-1}$  and  $0.017^\circ$ , respectively, during the experiments. Information about the functional groups and their arrangement in the glassy system of these samples were investigated by analyzing the Fourier transform infrared (FTIR) spectra. Fine powder samples were mixed with KBr, and then recorded spectrum was normalized to the spectrum of KBr.

**Table 2** The ashes of the agricultural wastes and eggshell powder in (wt%) along with their labels

Samples ID	SRE-1	SRE-2	SRE-3	SRE-4
Sugarcane leave ash	45	45	45	45
Rice husk ash	45	40	35	30
Eggshell powder	10	15	20	25

**Table 1** The chemical composition of the sugarcane leave ash and rice husk ash after heat-treatment at 1000 °C for 1 h

Chemical composition	SiO <sub>2</sub>	CaO	MgO	Na <sub>2</sub> O	K <sub>2</sub> O	Al <sub>2</sub> O <sub>3</sub>
Sugarcane leave ash (SCLA)	74.74	6.39	2.42	0.15	12.37	1.87
Rice husk Ash (RHA)	91	1.95	0.81	0.08	3.21	0.35
Eggshell powder (ESP)	0.54	98.18	0.41	0.41	-	0.46

FTIR spectra was checked using Perkin Elmer-Spectrum-RX-I FTIR spectrometer in the range 400–4000  $\text{cm}^{-1}$ . All the samples were examined by thermal gravimetric to check the stability of the samples. The experiment was performed on the heating rate with 10  $^{\circ}\text{C min}^{-1}$  in air. The samples were heat-treated at 900  $^{\circ}\text{C}$  for 10 h to study the crystalline phase formation and their effect on the coefficient of thermal expansion (CTE). CTE was done (DIL402PC, Netzsch) in air at a heating rate of 5  $\text{min}/^{\circ}\text{C}$ . The HITACHI U-3900 H double beam spectrophotometer used to diffuse reflectance UV/visible spectra were recorded within the spectral range 200–800 nm. Resolution and scanning speed of the instrument were 0.20 nm and 120  $\text{nm min}^{-1}$ . The optical band gap ( $E_g$ ), Urbach energy ( $E_U$ ) and refractive indexes were evaluated from the observed reflectance spectra. The luminescence behavior of the samples was analyzed by photoluminescence (PL). The room-temperature, PL excitation and emission spectra were recorded in the fluorescence mode with a fluorescence spectrophotometer (Model-Agilent Carry Eclipse G9800A, Mulgrave Melbourne, Australia) equipped with a xenon flash lamp. The wavelength corresponding to the maximum PL intensity of the excitation spectrum was observed from 235 to 265 nm.

## Result and discussion

### Elemental analysis

The ashes of various agro-food wastes are taken in wt% as given in Table 2. The EDS analysis is done to check the chemical composition of the as-quenched samples. It is given in Table 3. Interestingly, all the as-quenched samples contain  $\text{Al}_2\text{O}_3$ . The highest amount of  $\text{Al}_2\text{O}_3$  is found in SRE-4. It seems that this  $\text{Al}_2\text{O}_3$  picks up from the re-crystallized alumina crucible since samples are melted at high temperature 1550  $^{\circ}\text{C}$  in the re-crystallized alumina crucible. It seems that agro-food waste materials are more reactive as compared to conventional oxides of  $\text{SiO}_2$  and  $\text{CaO}$  [37]. It is associated with lower particle size than used mineral for glass formation.

It is observed that as eggshell content increases in initial composition (Table 1), the tendency of  $\text{Al}^{3+}$  diffusion is also increased from the crucible as shown in Table 3. The alkali and alkaline earth cations may have higher affinity towards

$\text{Al}^{3+}$  as compared to  $\text{Si}^{4+}$  cations. However, the ionic radii of  $\text{Si}^{4+}$  are much smaller than  $\text{Ca}^{2+}$  ions [38]. Moreover, the silicate is formed when the well-connected glass-network may decrease the possibility to react with  $\text{Al}_2\text{O}_3$  crucibles. On the other hand, most of the modifiers like  $\text{K}_2\text{O}$ ,  $\text{CaO}$  and  $\text{Na}_2\text{O}$  create non-bridging oxygen (NBOs), which may provide good sites for  $\text{Al}^{3+}$  diffusion and may form the bond with NBOs. The EDS analysis shows the systematic variation of  $\text{SiO}_2$  and  $\text{CaO}$  content. However,  $\text{K}_2\text{O}$ ,  $\text{MgO}$  and  $\text{Na}_2\text{O}$  could not show any ordered variation in their weight % as shown in Table 3.

### Density

The physical properties like density, molecular weight and molar volume are depending on the local structure of the glasses. In the silicate glasses, normally, density increases with increasing the atomic weight of the constituents [39]. Therefore, the increasing of ESP in initial constituents, increase the density and molecular weight from SRE-1 to SRE-4, which is given in Table 4. The density of the samples is also showing increasing trend. The density of the present glasses is comparable to other synthesized glasses by the minerals [37]. The molecular weight of constituent oxides in the present compositions follows the following trend;  $\text{Na}_2\text{O} < \text{K}_2\text{O} < \text{SiO}_2 < \text{MgO} < \text{CaO} < \text{Al}_2\text{O}_3$ . The modifier breaks the glass network led to the compactness of the glassy system. It is also reported by many researchers, when glasses were synthesized using the minerals [39]. At very high-temperature, where the melt is fluid, the melt consists of a eutectic mixture of modifier ions and various structural units of the network. They may be as small as the basic building block of the network or it may consist of a few of these building blocks connected to form small discrete ions of modifiers. When the melt is cooled rapidly, the network begins to form as the local structural units become connected. The alkaline earth metal or other modifier ions could break the connectivity of the glass network. A certain

**Table 4** Molecular weight and density of as-quenched samples

Sample ID	SRE-1	SRE-2	SRE-3	SRE-4
Molecular weight (g/mol)	61.38	61.36	61.69	62.31
Density (g/cc)	2.27	2.44	2.48	2.54

**Table 3** The chemical composition (wt%) of the as-quenched glasses calculated from EDS data

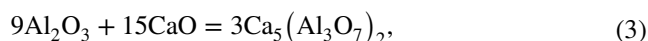
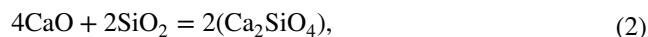
Samples ID	$\text{SiO}_2$	$\text{CaO}$	$\text{K}_2\text{O}$	$\text{MgO}$	$\text{Na}_2\text{O}$	$\text{Al}_2\text{O}_3$
SRE-1	81.85	8.02	4.77	3.59	0.45	1.32
SRE-2	78.37	12.76	4.38	2.66	0.09	1.74
SRE-3	74.98	15.05	3.68	2.90	0.00	2.22
SRE-4	69.91	18.36	4.34	2.51	0.35	4.52

amount of alkali and alkaline earth metals like  $K_2O$ ,  $Na_2O$ , and  $CaO$  always increase the density within the silicate glass system due to their molecular size and modifying behavior [40]. In addition to this,  $SiO_2$  and alkali/alkaline earth elements like  $MgO$ ,  $K_2O$  replaced by  $CaO$  result reduced the electrostatic forces between the kinds of non-bridging oxygen (NBO) considerably and hence decreases the characteristic temperature such glass transition temperature ( $T_g$ ), crystallization temperature ( $T_c$ ) of the glasses [39]. These modifiers have broken the network and increased the compactness of the system, which leads to decrease the molar volume of the glasses [41].

### X-ray diffraction

The X-ray diffraction patterns of the as-prepared and heat-treated samples are presented in Fig. 1a, b, respectively. A very broad hump is observed between  $2\theta = 17\text{--}35^\circ$ , which is associated with the amorphous characteristic of the as-quenched samples. The broad halo shifts towards the higher diffraction angle as  $SiO_2$  content decrease after adding the eggshell powder, which acted as a modifier. It may be associated with the higher number of non-bridging oxygen (NBO) and glass network connectivity and packing [39]. It is well reported that the modifiers break the network units and modify the packing of the different glass network, which influences the density of glasses. The higher amount of  $K_2O$ ,  $CaO$ ,  $Al_2O_3$  and other trace elements promote to disturb the connectivity of the glass network. SRE-4 has more modifying cation, hence, the viscosity is lower as compared to SRE-1. Therefore, as ESP increases, the glass formation tendency also increases

in the present samples. All the samples heat-treat at  $900^\circ C$  for 10 h to study the crystalline behavior of the glasses. SRE-1 sample exhibits two crystalline phases. These phases are formed accordingly to the given Eqs. (2), (3) and (4):



This sample forms the polymorphous phase of the silicate, i.e., stishovite phase  $SiO_2$  (ICDD No. 010-80-0371) and  $SiO_2$  phase (ICDD No. 010-82-1554). Whereas SRE-2 sample exhibits stishovite  $SiO_2$  (ICDD No. 01-081-1666) and calcium aluminum oxide  $CaAl_2O_4$  (ICDD No. 010-88-2477) with monoclinic structure. On the other hand, SRE-3 samples also show two crystalline phase, i.e, larnite  $Ca_2SiO_4$ , (ICDD No. 010-73-2091) with the monoclinic crystal structure and stishovite  $SiO_2$  (ICDD No. 010-80-0373)  $Ca_2SiO_4$  phase shows the phase transition at different temperature. SRE-4 sample shows higher crystallization tendency due to higher  $CaO$  and  $Al_2O_3$  content. In this sample, calcium silicate  $Ca_2(SiO_4)$  and calcium aluminum oxide  $Ca_5(Al_3O_7)_2$  (ICDD Nos. 01-087-1261 and 010-70-0801) crystalline phases are formed. The crystallization tendency of the heat-treated SRE-4 sample could be clearly seen in Fig. 1b. At the same time, the SRE-1 sample shows lower tendency of crystallization. All the samples are formed from the silicate-based crystalline phases. Additionally, SRE-2 and SRE-4 samples formed

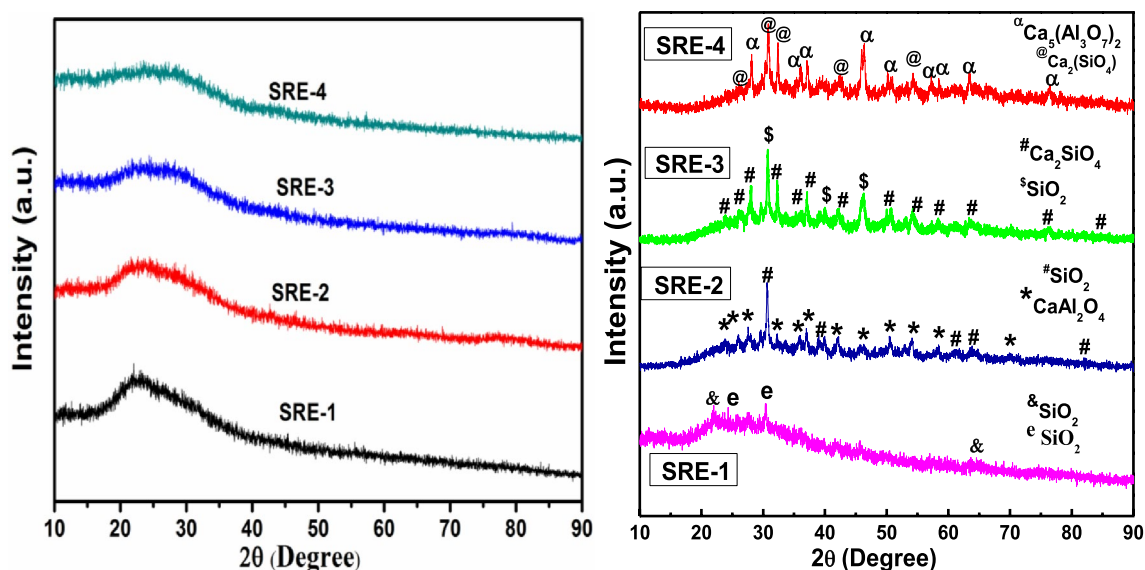


Fig. 1 XRD patterns of the SRE samples **a** as-quenched, **b** heat-treated at  $900^\circ C$  for 10 h

aluminates based phases. It is also reported by many researchers in the literature that in case of silicate-based glasses, during heat-treatment initially,  $\text{SiO}_2$  is nucleate that followed the diffusion of the modifier cations which lead to form the different crystalline phases [26]. In addition to this, it seems that intermediate oxides ( $\text{Al}_2\text{O}_3$ ) also acted as nucleating species to form aluminates related to crystalline phases. In all the four samples, the  $\text{Ca}_3\text{Al}_6\text{O}_{14}$  is a very good ionic conductor, as well as it exhibits excellent oxygen storage within nanocages in wide concentration range [9]. Therefore, this ceramic sample can be useful for electrolytes in fuel cell applications.

## FTIR analysis

FTIR spectra of the quenched samples are shown in Fig. 2. The FTIR result indicates that the intensity of these peaks is increased after adding ESP in initial constituents of the glasses. FTIR bands at  $\sim 2955\text{ cm}^{-1}$  belongs to Si–O–OH groups. The small kink is also observed at  $\sim 3688\text{ cm}^{-1}$ , particularly in the SRE-4 sample. These bands may belong to H–OH group. Both the bands are prominent only in the SRE-4 sample. The presence of hydroxyl group in this particular sample can be exploited for bioactive properties. Since,  $\text{OH}^-$  group always promote the hydroxyapatite layer formation during in vitro test [42]. The prominent and a broad band are observed at  $\sim 1000\text{ cm}^{-1}$ , which corresponds to various silicate units like  $\text{Q}_0$ ,  $\text{Q}_1$ ,  $\text{Q}_2$ ,  $\text{Q}_3$  and  $\text{Q}_4$ . As CaO increases in initial composition at a certain level, this band become diffuse up to SRE-3 clearly indicates the disturbance in the silicate glass network. Moreover, this bands shift towards lower wave number. It means the addition of ESP leads some modification in silicate units. The band becomes sharp in SRE-4 sample. It may be associated to some ordering that is taken place at the local level in this particular

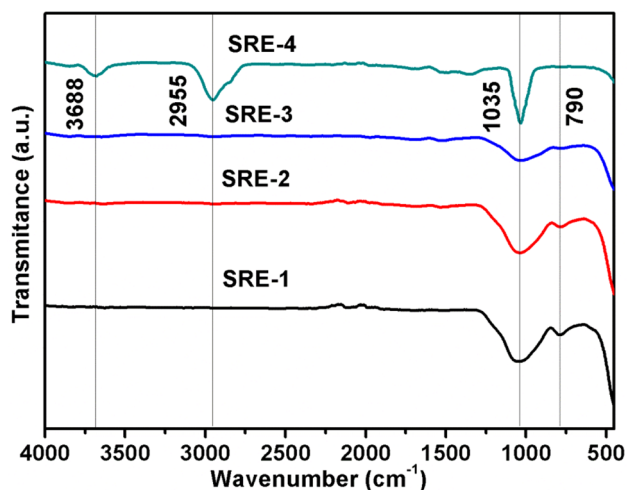


Fig. 2 FTIR spectra of the as-quenched glasses

glass. It is possible that even X-ray amorphous sample may have some crystalline or nanocrystalline phases in short range regions or sandwiched between two amorphous matrix [43]. The broadness of the band is due to the superposition of the IR-bands of the asymmetric vibrations of different type of Q-units of silica network. All molecules containing tetrahedral coordinated silicon are presented because this band becomes more intense and sharp in SRE-4 as compared to other samples. Therefore, it could be related to crystalline silicate network presented at the local level in this sample [44]. The band at  $\sim 790\text{ cm}^{-1}$  corresponds to the stretching vibrations of the silicate network, i. e., Si–O–Si bond vibrations [45].

## Thermal properties

### Thermogravimetric analysis

The TGA curve of the as-quenched samples is shown in Fig. 3. All the as-quenched samples show weight loss with minima at  $350\text{ }^\circ\text{C}$  except SRE-3 sample. SRE-3 sample shows the continuous weight loss up to  $900\text{ }^\circ\text{C}$ . However, initial weight loss is very steep up to  $350\text{ }^\circ\text{C}$  followed by  $0.5\%$  weight loss up to  $900\text{ }^\circ\text{C}$ . On the other hand, all other samples show weight loss up to  $350\text{ }^\circ\text{C}$  due to evaporation of crystalline water or trapped water in closed pores in the glasses. After that SRE-1, SRE-2 and SRE-4, glasses exhibit weight gain continuously. SRE-2 sample shows the highest weight gain  $\sim 1\%$  followed by SRE-1 and SRE-4 sample, respectively. In general, the weight gain is related to the oxidation of the transition metals. In the present samples, the transition metal oxides are not found as shown in Table 3. However, some trace transition metals are reported in the agricultural or food wastes, when these wastes analyzed by more sophisticated analysis

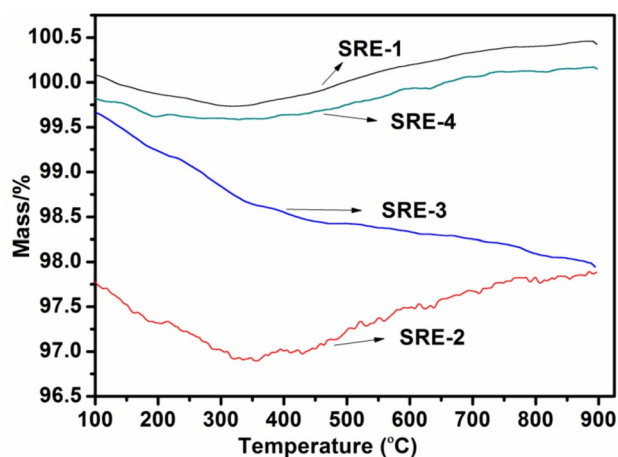
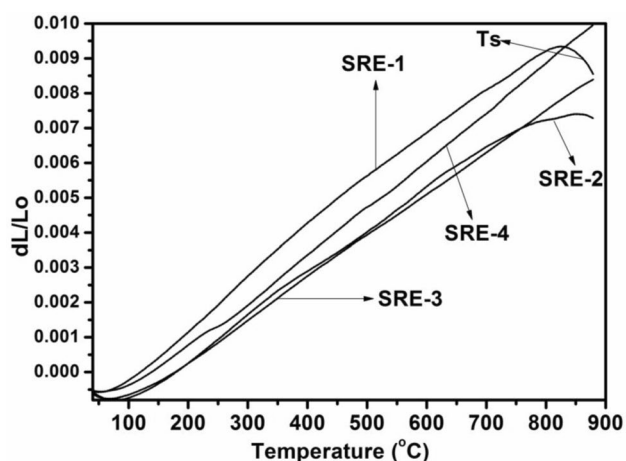


Fig. 3 Thermo gravimetric curves analysis of the SRE samples heated at  $10\text{ }^\circ\text{C min}^{-1}$  in air

techniques like MP-AES or ICP [46]. In contrast to other samples, SRE-3 shows different behavior, i.e., continuous weight loss in this particular sample is observed either it is related to some trace elements are reduced or loss of some organic contents, during the TG measurement. However, further and more sophisticated measurements are required to confirm the above interesting results. For the thermal stability point of view, the SRE-4 sample is more stable than the other samples. Moreover, the thermal stability of the present samples (derived from wastes) is comparable with those glasses synthesized by normal chemicals (minerals) for similar compositions [47].



**Fig. 4** The coefficient of thermal expansion of glass–ceramics samples after sintering the pellets at 900 °C for 10 h

### Dilatometric analysis

The coefficient of thermal expansion (CTE) is calculated on the heat-treated samples at 900 °C for 10 h. The thermal expansion curves of heat-treated samples are shown in Fig. 4. The addition of eggshell (CaO) act as a modifier and then it creates more non-bridging oxygen (NBO) in the samples, which affects the stabilization of glass-network to decrease the characteristic glass-transition temperatures. The heat-treated SRE-4 sample shows the deviation at 260 °C. It may be related to the phase transition. The crystalline phase  $\text{Ca}_5\text{Al}_6\text{O}_{14}$  exhibit phase transition as reported by [26]. The SRE-1 and SRE-2 show the softening temperature at  $\sim 800$  °C, which clearly indicate that, some glassy matrix still present in these samples, even after heat-treatment. SRE-3 and SRE-4, glasses show higher tendency to grow the crystalline phase become glass–ceramics as compared to SRE-1 and SRE-2, samples. SRE-1 sample also shows higher slope that indicates higher CTE of this sample as compared to the other samples. The replacement of RHA by eggshell powder, at a particular level in the samples, is in support to enhance the crystallization tendency of the glasses as also observed in XRD Fig. 3b. The properties of the glasses and glass–ceramics could be tailored to select proper agro-food wastes. SRE-3 and SRE-4 samples show remarkable thermal stability up to 900 °C. It is comparable with glasses, which are synthesized with minerals [37].

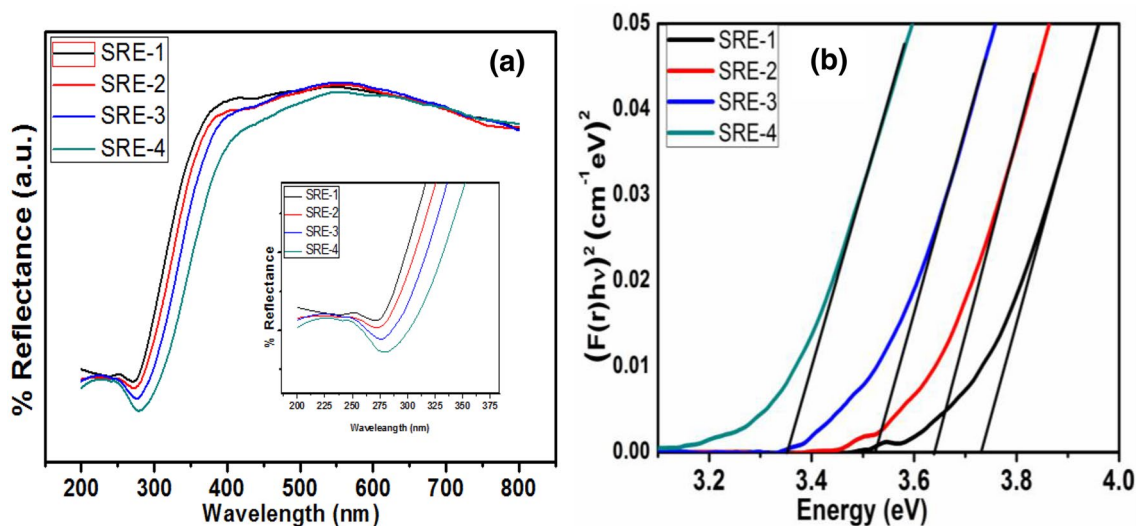


**Fig. 5** a Reflectance and 5 (b) Tauc's plot of the as-quenched samples

## UV/visible analysis

### Optical band gap and Urbach energy

Diffused reflectance spectra of the as-quenched glasses are shown in Fig. 5. The signature of phase separation phenomena in the glasses could be established by the UV/visible spectra. A kink at ~262 nm is clearly seen in all the glasses. This kink might be originated due to the presence of a different glass matrix within the glass matrix, i. e. phase separated glass. From spectra, the optical band gaps of the as-quenched glasses were calculated using Kubelka–Munk function [48] reported elsewhere [32]. Tauc's plot shown in Fig. 5b, ensures optical band gap decreases trend with increasing ESP content. Maximum optical band gap (3.72 eV) is shown in SRE-1 sample. The minimum value of band gap is measured in SRE-4 sample due to the RHA is replaced by ESP (wt%). These values are comparable to the silicate-rich glasses as synthesized by mineral route [35]. Band gap of all the samples lies into insulator region. Usually, NBO's is responsible to vary the band gap in the glasses. After increasing the modifiers content, band gap decreases, this expected trend is also followed in the present samples. A kink is observed in agro-food wastes, which become diffuse due to higher amount of CaO. In addition to this, phase separation tendency decreased by the addition of ESP in the present glasses. It clearly indicates that the phase separation tendency decreases and Urbach energy increases by the addition of ESP in initial composition.

### Refractive index

The refractive indexes of the glasses are determined by the interaction of light with the electrons of its glass constituents and other details related to optical properties are given elsewhere [36]. Normally, the covalent character of the bonds and difference in the electro-negativities of the bond forming influenced the refractive index. Additionally, it also depends on the NBO's created by adding of different modifiers. The increasing trends of the percentage of the covalent character of the bonds are following this sequence  $\text{SiO}_2 > \text{CaO} > \text{K}_2\text{O}$ , etc, whereas in  $\text{K}_2\text{O}$  bond, refractive index also decreases with decreasing covalent bond character. The variation of the covalent character of the bonds is responsible to vary the refractive index. However, the refractive index is shown as increasing trend in all the samples after increasing the ESP (CaO). ESP rich modifier creates non-bridging oxygen's (NBO), which is more polarizable than bridging oxygen. Therefore, the formation of the non-bridging oxygen increases the refractive index of the glasses. Therefore, refractive index ( $n$ ) is higher in SRE-4 with maximum ESP containing glass in comparison to other samples. Although, the formation of partial crystalline phases may affect the refractive index of the samples.

**Table 5** Optical band gap, refractive index and Urbach energy along with their samples labels

Samples ID	SRE-1	SRE-2	SRE-3	SRE-4
Optical band gap (eV)	3.72	3.60	3.51	3.34
Refractive index (n)	2.23	2.25	2.27	2.31
Urbach energy ( $E_U$ ) eV	0.29	0.30	0.32	0.34

However, the covalent character and polarizability have been the dominating factors to influence the refractive index of the as-quenched samples. For calculating the Urbach energy ( $E_U$ ) of all samples details are given somewhere else [32]. All the values like optical band gap and Urbach energy are shown in Table 5. The Urbach energy increases with increasing ESP in the agricultural waste based samples. Actually, RHA is having maximum  $\text{SiO}_2$ , which act as a glass matrix with the small amount of alkali and alkaline earth metals and these trace elements can act as the modifiers as well as the network former [46]. However, in the given samples, modifiers contents are higher in the SRE-4 sample due to the higher ESP amount. Conclusively, covalent character, plausibility and NBO's play important role to decide the values of band gap and Urbach energy in these samples.

### Photoluminescence

In the present study, the as-quenched glasses are heat-treated at 900 °C for 10 h then photoluminescence (PL) spectra recorded in the region of 300–500 nm. In this region, it exhibits strong, medium and weak intensity peaks. These peaks lie in the blue to the green spectral region. All the prepared glasses show high refractive index ( $n \sim 2.31$ ) and good transparency (T-80%) in the UV–visible ( $\lambda$ -235 nm) and near-infrared range. In more complex silicate glasses, luminescence can be promoted by the incorporation of several alkaline and rare earth ions, but the concentrations are usually effective due to heavy elements in these glasses. Impurities have been identified in silicate glasses by luminescent effects atomic concentration levels, which produce undetectable optical absorption [32, 49]. PL spectra are shown on the pellet of four samples sintered at 900 °C for 10 h in Fig. 6. The UV–Vis–NIR absorption spectrum reveals several peaks centered at excitation of electron from ground state  $4I_{9/2}$  to  $4D_{3/2} + 4D_{5/2}$  (360 nm),  $2G_{9/2} + 2D_{3/2} + 2P_{3/2}$  (485 nm). It is clearly observed that emission consists apparently of many broad bands at 360–364 nm, 369–373 nm, 408 nm, 421–423 nm, 446 nm and 484–485 nm also shifted to the right side for all the samples [40]. At 360–373 nm peaks observed in UV–visible region due to the exceeding defects of Si- and oxygen defect center (ODC), the singlet–singlet transition of Si-divalent of  $\text{Ca}^{2+}$  [41]. Consequently, an investigation of the source of this luminescence was undertaken.

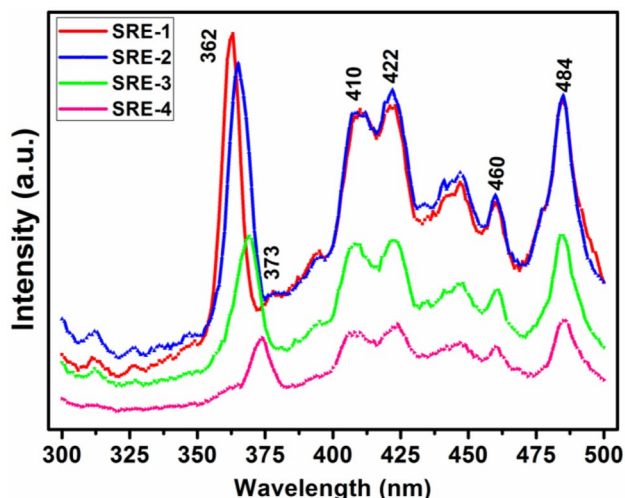


Fig. 6 Photoluminescence behavior of the as-quenched glasses

Weak luminescence is observed in many glasses, but in the present samples, the PL sources are not generally understood. A blue luminescence in silicate glasses has been ascribed due to traces of elements. Emission band at 421 nm show blue shift due to self-trapped exciton (STE) associated with  $\text{Al}^{3+}$  and creation of  $=\text{O}-\text{O}=\text{O}$  bond and ODC.

It is also affected with enhancing intrinsic defects, which was found due to the presence of dopants or impurity in the glass. The green region also observed at 485 nm, which is directly influenced by  $\text{Al}^{3+}$ ,  $\text{Na}^+$ ,  $\text{K}^+$ , and  $\text{Ca}^{2+}$  implantations ODC or  $\text{Al}^{3+}$ -centre impurity incorporation during growth or Ca–O valance-related defects attached with the triplet–singlet emission of Ca–O valency [32, 50, 51]. In the present samples, as crystallization increases from SRE-1 to SRE-4 as discussed in XRD section, the intensity of PL emission spectra increases as eggshell content increase and shift towards to lower wavelength blue shift particularly bands at 300–380 nm. Conclusively, higher wavelength PL peaks are not shifted with respect to ESP content except peaks at 375–362 nm. The PL of the silicon clusters has potential applications in Si-based optoelectronic devices, especially in green–blue and UV luminescence devices. Moreover, these glasses and glass–ceramics could be used in the continuous as well as pulsed laser applications.

## Conclusions

The agro-food wastes are successfully used as resource materials to synthesize glasses. After heat-treatment different crystalline phases are formed in heat-treated glasses. The density and molar weight of the glasses increases with eggshell content. The replacement of RHA by eggshell powder enhanced the crystallization tendency of the glasses. SRE-3 and SRE-4 show remarkable thermal stability up to 900 °C. Optical band gap

value lies in the range of wide band gap semiconductor, i.e., 3.34–3.72 eV. The PL intensity increases as eggshell content decrease. It shifts towards to lower wavelength particularly bands at 300–380 nm. These glasses and glass–ceramics may find application in the continuous as well as pulsed lasers.

**Acknowledgements** The authors are very grateful to Santhosh Kumar Mahadevan and Dr. Jayant Kolte for their valuable suggestion and SAI labs, TIET, Patiala for providing characterization facilities. Authors are thankful to Dr. Sanjay Sharma (Modi College, Patiala) for their help in FTIR results.

## References

- Liu N, Huo K, McDowell MT, Zhao J, Cui Y (2013) Rice husks as a sustainable source of nanostructured silicon for high performance Li-ion battery anodes. *Sci Rep* 3:1–7. <https://doi.org/10.1038/srep01919>
- Mohanta K, Kumar D, Parkash O (2012) Properties and Industrial applications of rice husk: a review. *Int J Emerg Technol Adv Eng* 2:86–90
- Wang Y, Zhao Q, Han N, Bai L, Li J, Liu J, Che E, Hu L, Zhang Q, Jiang T, Wang S (2015) Mesoporous silica nanoparticles in drug delivery and biomedical applications, *Nanomedicine Nanotechnology Biol Med* 11:313–327. <https://doi.org/10.1016/j.nano.2014.09.014>
- Abdulrahman I, Tijani HI, Mohammed BA, Saidu H, Yusuf H, Jibrin MN, Mohammed S (2014) From garbage to biomaterials: an overview on eggshell based hydroxyapatite. *J Mater Sci* 2014:6. <https://doi.org/10.1155/2014/802467>
- Adam F, Nelson J, Khanam Z, Thankappan R, Asri M, Nawi M (2013) Applied surface science utilization of tin and titanium incorporated rice husk silica nanocomposite as photocatalyst and adsorbent for the removal of methylene blue in aqueous medium. *Appl Surf Sci* 264:718–726. <https://doi.org/10.1016/j.apsusc.2012.10.106>
- Haslinawati MM, Matori KA, Waheb ZA, Sidek HAA, Zainal AT (2009) Effect of temperature on ceramic from rice husk ash. *Int J Basic Appl Sci* 9:1–3
- Lee T, Othman R, Yeoh FY (2013) Development of photoluminescent glass derived from rice husk. *Biomass Bioenergy* 59:380–392. <https://doi.org/10.1016/j.biombioe.2013.08.028>
- Aktas B, Albaskar M, Yalcin S, Dogru K (2016) Optical properties of soda-lime-silica glasses doped with peanut shell powder. *Arch Mater Sci Eng* 82:57–61
- Firihu MZ (2017) Characteristic of silica xerogel from rice husk ash wastes sintered by microwave and conventional. *Pure Appl Chem Sci* 5:1–7
- Pode R (2016) Potential applications of rice husk ash waste from rice husk biomass power plant. *Renew Sustain Energy Rev*. <https://doi.org/10.1016/j.rser.2015.09.051>
- Vijayakumar K, Safai PD, Devara PCS, Rao SVB, Jayasankar CK (2016) Effects of agriculture crop residue burning on aerosol properties and long-range transport over northern India: a study using satellite data and model simulations. *Atmos Res* 178:155–163. <https://doi.org/10.1016/j.atmosres.2016.04.003>
- Chaow-u-thai A, Inthidech S, Rittidech S, Pattiya A (2012) Removal of ash from sugarcane leaves and tops. *Int J Bio Sci* 2:12–17
- Binod P, Sindhu R, Singhanian RR, Vikram S, Devi L, Nagalakshmi S, Kurien N, Sukumaran RK, Pandey A (2010) Bioethanol production from rice straw: an overview. *Bioresour Technol* 101:4767–4774



14. Rashad A (2016) Cementitious materials and agricultural wastes as natural fine aggregate replacement in conventional mortar and concrete. *J Build Eng* 5:119–141. <https://doi.org/10.1016/j.jobte.2015.11.011>
15. Shrivastava A, Ash F (2015) Application of different waste in concrete as a partial replacement of cement coarse aggregate. *Int J Sci Tech Eng* 2:89–107
16. Singh M, Siddique R (2013) Resources, conservation and recycling effect of coal bottom ash as partial replacement of sand on properties of concrete. *Resources Conserv Recycl* 72:20–32. <https://doi.org/10.1016/j.resconrec.2012.12.006>
17. Ogunribido THT, MNMGS MTRCN (2011) Potentials of sugar cane straw ash for lateritic soil stabilization in road construction. *Int J Sci Emerg Technol* 3:102–106
18. Kumar A, Sengupta B, Dasgupta D, Mandal T, Datta S (2016) Recovery of value added products from rice husk ash to explore an economic way for recycle and reuse of agricultural waste. *Rev Environ Sci Biotechnol*. <https://doi.org/10.1007/s11157-015-9388-0>
19. Anshar M, Ani FN, Kader AS (2016) Electrical energy potential of rice husk as fuel for power generation in Indonesia. *ARPN J Eng Appl Sci* 11: 3616–3624
20. Regis M, Leal LV, Galdos MV, Walter A, Oliveira COF (2013) Sugarcane straw availability, quality, recovery and energy use: a literature review. *Biomass Bioenerg*. <https://doi.org/10.1016/j.biombioe.2013.03.007>
21. Nagrale SD, Hajare H, Modak PR (2012) Utilization of rice husk ash. *Int J Eng Res Appl* 2:1–5
22. Devi L, Jayasankar CK (2018) Spectroscopic investigations on high efficiency deep red-emitting  $\text{Ca}_2\text{SiO}_4:\text{Eu}^{3+}$  phosphors synthesized from agricultural waste. *Ceram Int*. <https://doi.org/10.1016/j.ceramint.2018.05.003>
23. Baláž M (2014) Eggshell membrane biomaterial as a platform for applications in materials science. *Acta Biomater* 10:3827–3843. <https://doi.org/10.1016/j.actbio.2014.03.020>
24. Oliveira DA, Benelli P, Amante ER (2013) A literature review on adding value to solid residues: egg shells. *J Clean Prod* 46:42–47. <https://doi.org/10.1016/j.jclepro.2012.09.045>
25. Cornejo IA, Ramalingam S, Fish JS, Reimanis IE (2014) Hidden treasures: TURNING food waste into glass. *Amer Ceram Soc Bull* 93:24–27
26. Lahl N, Bahadur D, Singh K, Singheiser L, Hilpert K (2002) Chemical interactions between aluminosilicate base sealants and the components on the anode side of solid oxide. *Fuel Cells* 149:607–614. <https://doi.org/10.1149/1.1467945>
27. Jha P, Danewalia SS, Sharma G, Singh K (2018) Antimicrobial and bioactive phosphate-free glass–ceramics for bone tissue engineering applications. *Mater Sci Eng C* 86:9–17. <https://doi.org/10.1016/j.msec.2018.01.002>
28. Lee T, Othman R, Yeoh FY (2013) Development of photoluminescent glass derived from rice husk. *Biomass Bioenerg* 59:380–392. <https://doi.org/10.1016/j.biombioe.2013.08.028>
29. Siegel GJ (1974) Ultraviolet spectra of silicate glasses: a review of some experimental evidence. *J Non Cryst Solids* 13(74):372–398. [https://doi.org/10.1016/0022-3093\(74\)372-7](https://doi.org/10.1016/0022-3093(74)372-7)
30. Barbieri L, Ferrari AM, Lancellotti I, Leonelli C, Rincón JM, Romero M (2004) Crystallization of  $(\text{Na}_2\text{O}-\text{MgO})-\text{CaO}-\text{Al}_2\text{O}_3-\text{SiO}_2$  glassy systems formulated from waste products. *J Am Ceram Soc* 83:2515–2520. <https://doi.org/10.1111/j.1151-2916.2000.tb01584.x>
31. Chuayjuljit S, Eiumnoh S, Potiyaraj P (2001) Using silica from rice husk as a reinforcing filler in natural rubber. *J Sci Res Chula Univ* 26:127–138
32. Wang S (2008) Application of solid ash based catalysts in heterogeneous catalysis. *Environ Sci Technol* 42:7055–7063. <https://doi.org/10.1021/es801312m>
33. Sharma G, Arya SK, Singh K (2018) Optical and thermal properties of glasses and glass-ceramics derived from agricultural wastes. *Ceram Int* 44:947–952. <https://doi.org/10.1016/j.ceramint.2017.10.027>
34. Chandrasekhar S, Satyanarayana KG, Pramada PN, Raghavan P, Gupta TN (2003) Processing, properties and applications of reactive silica from rice husk—an overview. *J Mat Sci* 38:3159–3168. <https://doi.org/10.1023/A:1025157114800>
35. Yasothai R, Kavitha NV (2014) Eggshell waste is a calcium source for layers: review. *Int J Sci Environ Technol* 3:1465–1471
36. Singh S, Singh K (2015) Nanocrystalline glass ceramics: structural, physical and optical properties. *J Mol Struct* 1081:211–216. <https://doi.org/10.1016/j.molstruc.2014.10.018>
37. Jha P, Singh K (2015) Effect of MgO on bioactivity, hardness, structural and optical properties of  $\text{SiO}_2-\text{K}_2\text{O}-\text{CaO}-\text{MgO}$  glasses. *Ceram Int* 42:436–444. <https://doi.org/10.1016/j.ceramint.2015.08.128>
38. Shannon RD (1993) Dielectric polarizabilities of ions in oxides and fluorides. *J Appl Phys* 73:348–366. <https://doi.org/10.1063/1.353856>
39. Shelby JE (2005) Introduction to glass science and technology. Royal Society of Chemistry, Cambridge
40. Ingwell DOB (1999) Densities of melts in the  $\text{CaO}-\text{MgO}-\text{Al}_2\text{O}_3-\text{SiO}_2$  system. *Am Mineral* 84:465–476
41. Danewalia SS, Singh K (2016) Magnetic and bioactive properties of  $\text{MnO}_2/\text{Fe}_2\text{O}_3$  modified  $\text{Na}_2\text{O}-\text{CaO}-\text{P}_2\text{O}_5-\text{SiO}_2$  glasses and nanocrystalline glass-ceramics. *Ceram Int* 42:11858–11865. <https://doi.org/10.1016/j.ceramint.2016.04.108>
42. Singh K, Bala I, Kumar V (2009) Structural, optical and bioactive properties of calcium borosilicate glasses. *Ceram Int*. <https://doi.org/10.1016/j.ceramint.2009.06.006>
43. Kaur G, Pandey OP, Singh K (2012) Effect of modifiers field strength on optical, structural and mechanical properties of lanthanum borosilicate glasses. *J Non Cryst Solids* 358:2589–2596. <https://doi.org/10.1016/j.jnoncrysol.2012.06.006>
44. Kalampounias AG (2011) IR and Raman spectroscopic studies of sol–gel derived alkaline-earth. *Bull Mat Sci* 34:299–303
45. Zamratul MIM, Zaidan AW, Khamirul AM, Nurzilla M, Halim SA (2016) Results in physics formation, structural and optical characterization of neodymium doped-zinc soda lime silica based glass. *Res Phys* 6:295–298
46. Danewalia SS, Sharma G, Thakur S, Singh K (2016) Agricultural wastes as a resource of raw materials for developing low-dielectric glass–ceramics. *Sci Rep* 6:24617. <https://doi.org/10.1038/srep24617>
47. Fluegel A (2007) Thermal expansion calculation of silicate glasses at 210. *Most* 60:1–25
48. Kubelka P, Munk F (1931) Ein Beitrag zur Optik der Farbanstriche. *Zeitschrift für Tech Phys* 12:593–601. <https://doi.org/10.4236/msce.2014.28004>
49. Kaviyarasu K, Manikandan E, Kennedy J, Jayachandran M, Maaza M (2016) Rice husks as a sustainable source of high quality nanostructured silica for high performance Li-ion battery. *Adv Mats Lett*. <https://doi.org/10.5185/amlett.2016.6192>
50. Salh R (2011) Defect related luminescence in silicon dioxide network: a review. *Cryst Silicon Prop Uses*. <https://doi.org/10.5772/22607>
51. Imai H, Arai K, Imagawa H, Hosono H, Abe Y (1988) Two types of oxygen-deficient centers in synthetic silica glasses. *Phys Rev B* 38:772–775